

# Observational constraints on a holographic, interacting dark energy model

Iván Durán\*,<sup>1</sup> Diego Pavón†,<sup>2</sup> and Winfried Zimdahl‡<sup>3</sup>

<sup>1</sup>*Departamento de Física, Universidad Autónoma de Barcelona, 08193 Bellaterra (Barcelona), Spain.*

<sup>2</sup>*Departamento de Física, Universitat Autònoma de Barcelona, 08193 Bellaterra (Barcelona), Spain.*

<sup>3</sup>*Departamento de Física, Universidade Federal do Espírito Santo, Brasil.*

## Abstract

We constrain an interacting, holographic dark energy model, first proposed by two of us in [1], with observational data from supernovae, CMB shift, baryon acoustic oscillations, x-rays, and the Hubble rate. The growth function for this model is also studied. The model fits the data reasonably well but still the conventional  $\Lambda$ CDM model fares better. Nevertheless, the holographic model greatly alleviates the coincidence problem and shows compatibility at  $1\sigma$  confidence level with the age of the old quasar APM 08279+5255.

---

\* E-mail: ivan.duran@uab.cat

† E-mail: diego.pavon@uab.es

‡ E-Mail: winfried.zimdahl@pq.cnpq.br

## I. INTRODUCTION

Models of holographic dark energy have become popular as they rest on the very reasonable assumption that the entropy of every bounded region of the Universe, of size  $L$ , should not exceed the entropy of a Schwarzschild black hole of the same size. That is to say,

$$L^3 \Lambda^3 \leq S_{BH} \simeq L^2 M_{Pl}^2 \quad (M_{Pl}^2 = (8\pi G)^{-1}), \quad (1)$$

where  $\Lambda$  stands for the ultraviolet cutoff, the infrared cutoff is set by  $L$ .

However, as demonstrated by Cohen *et al.* [2], an effective field theory that saturates the above inequality necessarily includes states for which the Schwarzschild radius exceeds  $L$ . It is therefore natural to replace the said bound by another one that excludes such states right away, namely,

$$L^3 \Lambda^4 \leq M_{Pl}^2 L. \quad (2)$$

This bound guarantees that the energy  $L^3 \Lambda^4$  in a region of the size  $L$  does not exceed the energy of a black hole of the same size [3]. By saturating the inequality (2) and identifying  $\Lambda^4$  with the density of holographic dark energy,  $\rho_X$ , it follows that [2, 3]

$$\rho_X = \frac{3c^2}{8\pi G L^2}, \quad (3)$$

where the factor 3 was introduced for convenience and  $c^2$  is a dimensionless quantity, usually assumed constant, that collects the uncertainties of the theory (such as the number particle species and so on). For a more thorough motivation of holographic dark energy see Section 3 of [1].

Last relationship is widely used in setting models of holographic dark energy that aim to explain the present stage of cosmic accelerated expansion, [4–7], via the huge negative pressure associated to them. Broadly speaking holographic dark energy models fall into three main groups depending on the choice of the infrared cutoff,  $L$ . Namely, the Hubble radius [1, 8], the event horizon radius [3, 9–13], and the Ricci’s length [14–17]. The particle horizon radius was also used [18] but it presents the severe drawback of leading to a cosmology incompatible with a transition from deceleration to acceleration during the Universe expansion.

In this paper we consider a spatially flat Friedmann- Robertson-Walker universe dominated by holographic dark energy (with the infrared cutoff set by the Hubble radius, i.e.,  $L = H^{-1}$ ) and pressureless dark matter such that these two components are dynamically linked by an interaction term. The model was introduced in [1]. Here we constrain it with data from supernovae type Ia (SN Ia), the shift of the first acoustic peak in the cosmic background radiation (CMB shift),

baryon acoustic oscillations (BAO), and x-rays (strongly related to the baryon gas abundance in galaxy clusters), and Hubble's history,  $H(z)$ . We also study the evolution of the growth function which potentially may constrain the model as well. But we do not use them because, at present, these data are far noisier than those in the other data sets.

The paper is organized as follows. Section II recalls the holographic interacting model. Section III constrains the model with observational data. Notwithstanding it does not contain the flat  $\Lambda$ CDM model as a limiting case (at variance with, e.g., quintessence models) it shows a sizable overlap with the latter. Section IV studies the growth function. Finally, Section V summarizes our overall conclusions. As usual, a zero subindex indicates the present value of the corresponding quantity.

## II. BASICS OF THE MODEL

The spatially flat FRW holographic model proposed in [1] rests on two main assumptions: (i) The dark energy density is governed by the saturated holographic relationship, Eq. (3), with the infrared cutoff fixed by the Hubble radius, i.e.,  $L = H^{-1}$ . (ii) Dark matter and dark energy do not evolve independently of each other. They interact according to

$$\dot{\rho}_M + 3H\rho_M = Q, \quad \text{and} \quad \dot{\rho}_X + 3H(1+w)\rho_X = -Q, \quad (4)$$

where  $w = p_X/\rho_X$  stands for the equation of state parameter of dark energy, and

$$Q = \Gamma \rho_X \quad (5)$$

is the interaction term where  $\Gamma$  denotes the rate by which  $\rho_X$  changes as a result of the interaction. We assume  $\Gamma$  to be semipositive-definite. Note that if  $Q$  were negative, the transfer of energy would go from dark matter to dark energy, in contradiction with the second law of thermodynamics [19]. Further, use of the Layzer-Irvine equation on nearly one hundred galaxy clusters strongly supports this view [20].

Interacting models were first proposed by Wetterich to lower down the value of the cosmological term [21]. Later on it was proved efficient in easing the cosmic coincidence problem [22, 23] and it was suggested that the interaction (whatever form it might take) is not only likely but inevitable [24, 25]. The amount of literature on the subject is steadily increasing -see, e.g., [26] and references therein. Admittedly, the expression (5) is nothing but a useful parametrization of the interaction. Given our poor understanding of the nature of dark matter and dark energy, there is no clear

guidance to derive an expression for  $Q$  from first principles. This is why our approach will be purely phenomenological.

The model is fully specified by three quantities, e.g., the current value of the Hubble rate,  $H_0$ , the dimensionless density parameter  $\Omega_X := 8\pi G\rho_X/(3H^2)$  (or, equivalently,  $\Omega_M$ ), and  $\Gamma$ . Note that  $c^2$  is fixed by  $c^2 = \Omega_X$ , as it can be readily checked.

The first assumption readily implies that  $\Omega_X$  does not vary with expansion, and that the ratio of energy densities,  $r := \rho_M/\rho_X$ , stays fixed in spatially flat FRW universes ( $\Omega_M + \Omega_X = 1$ ) for any interaction. The latter consequence greatly alleviates the coincidence problem albeit, strictly speaking, it does not solve it in full because the model cannot predict that  $r \sim \mathcal{O}(1)$  (to the best of our knowledge, no model is able to predict that). This feature of  $\Omega_X$  and  $r$  being strictly constants may seem too strong; however, one should bear in mind that both quantities would slightly vary with the Universe expansion if the parameter  $c^2$  in Eq. (3) were allow to weakly depend on time, something not at all unreasonable. Further,  $r$  would not be constant if the restriction to spatial flatness were relaxed. At any rate, we shall take the conservative stance that both  $c^2$  and  $r$  do not vary; thus, the number of free parameters of the model will be kept to a minimum.

At first sight, the consequence of  $\Omega_X$  being of order unity also at early times might look worrisome. One may think that a large dark energy component at that period would prevent the formation of gravitationally bound objects. However, this is not the case as

$$w = -\frac{1+r}{r} \frac{\Gamma}{3H} \quad (6)$$

is not constant, and for suitable choice of the ratio  $\Gamma/H$  it tends to the equation of state of non-relativistic matter at early times. Its evolution is governed by the Hubble rate which, in the simplest case of  $\Gamma$  being a constant, takes the form

$$H = H_0 \left[ \frac{\Gamma}{3H_0 r} + \left( 1 - \frac{\Gamma}{3H_0 r} \right) a^{-3/2} \right], \quad (7)$$

which corresponds to a specific generalized Chaplygin gas [27]. In last expression, the scale factor has been normalized by setting  $a_0 = 1$ . Figures 1 and 2 show the history of the equation of state for the best fit values of the model up to redshifts 8 and 1.2, respectively. Figure 1 illustrates that at high redshifts  $w$  approaches zero asymptotically. Figure 2 shows that, in accordance with the analysis in [28],  $w(z)$  varies little at small redshifts.

The deceleration parameter,  $q := -\ddot{a}/(aH^2)$ , whose evolution is illustrated in Fig. 3, obeys

$$q = \frac{1}{2} \left( 1 - \frac{\Gamma}{Hr} \right). \quad (8)$$

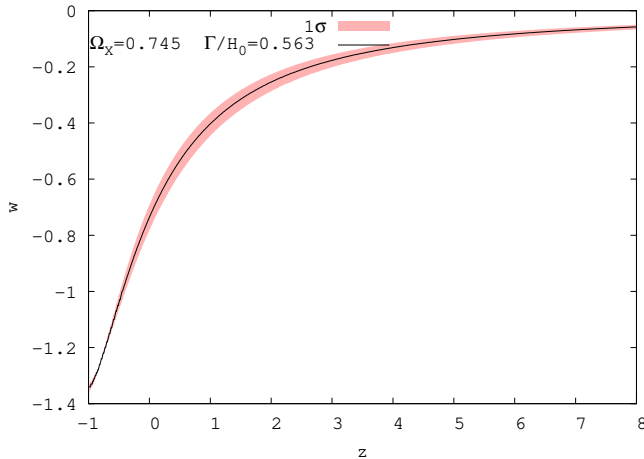


Figure 1: Evolution of the equation of state parameter of dark energy, Eq. (6), for the best fit model, up to  $z = 8$ . In this, as well as in subsequent figures, the red swath indicates the region obtained by including the  $1\sigma$  uncertainties of the constrained parameters used in the calculation (in the present case,  $\Omega_X$  and  $\Gamma/H_0$ ).

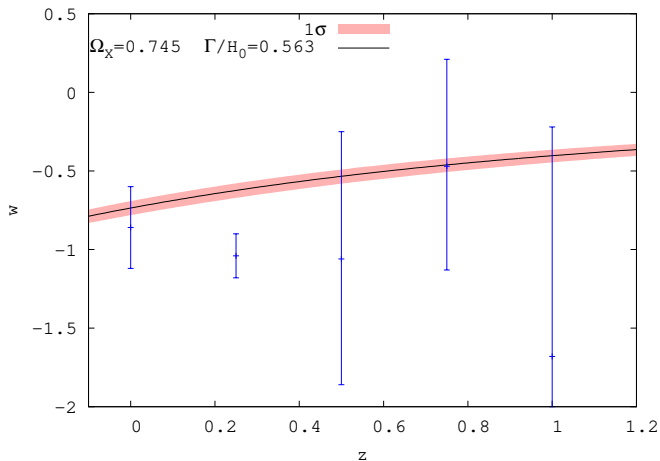


Figure 2: Evolution of the equation of state of dark energy for the best fit model up to  $z = 1.2$ . The observational data with their  $2\sigma$  error bars are borrowed from [28]. In plotting the curve no fit to these data was made.

This expression implies that  $q \rightarrow \frac{1}{2}$  at high redshifts as it should, and that the transition from deceleration to acceleration occurs at

$$z_{tr} = \left( \frac{2\Gamma}{3H_0 r - \Gamma} \right)^{2/3} - 1, \quad (9)$$

which yields  $z_{tr} \simeq 0.80$  for the best fit values. It should be noted that in [8] the transition deceleration-acceleration required that the  $c^2$  varied, if only very slowly. In the present case, the

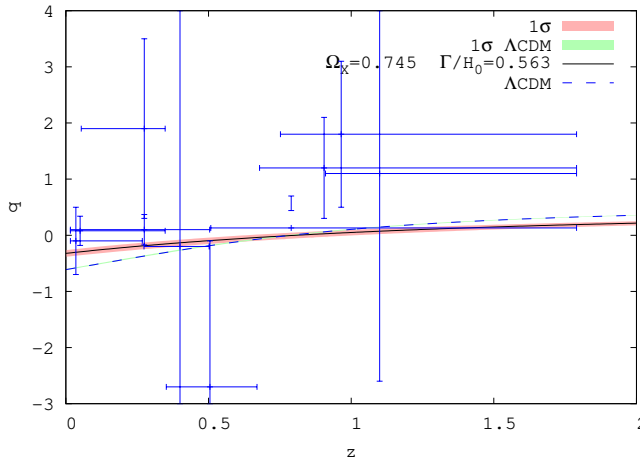


Figure 3: History of the deceleration parameter, according to Eq. (8) in terms of redshift for the best fit holographic model (solid line). The redshift at which the transition deceleration-acceleration occurs is approximately 0.80. Also shown is the prediction of the  $\Lambda$ CDM model (dashed line). In this, as well as in subsequent figures, the green swath indicates the region obtained by including the  $1\sigma$  uncertainties of the constrained parameters used in the calculation (in the present case just  $\Omega_{M0}$ ). The data are borrowed from [29]. In drawing the curves no fit to these data was made.

transition also occurs for  $c^2 = \text{constant}$  (as, for simplicity, we are considering). The difference stems from the fact that in [8] the ratio  $\Gamma/H$  was kept constant, while the present model has  $\Gamma = \text{constant}$ , instead.

The age of old luminous objects at high redshifts can constrain cosmological models by simply requiring that their age at the redshift they are observed do not exceed the age of the Universe at that redshift. Figure 4 depicts the dependence of the age of the Universe on redshift for the best fit values of both the holographic model and the  $\Lambda$ CDM model alongside the age and redshift of three luminous old objects, namely: galaxies LBDS 53W069 ( $z = 1.43$ ,  $t = 4.0$  Gyr) [30] and LBDS 53W091 ( $z = 1.55$ ,  $t = 3.5$  Gyr) [31, 32], as well as the quasar APM 08279+5255 ( $z = 3.91$ ,  $t = 2.1$  Gyr) [33, 34]. While the ages of the two first objects are lower than the ages of the holographic model and the  $\Lambda$ CDM model at the corresponding redshifts, the age of the quasar APM 08279+5255 lies slightly further than  $1\sigma$  beyond the age of the  $\Lambda$ CDM model at  $z = 3.91$ . By contrast, the holographic model is compatible at  $1\sigma$  level with the age of the said quasar. The tension between the APM quasar and the  $\Lambda$ CDM model has been known for some time now (see [34] and references therein) and it has been revisited recently [35, 36].

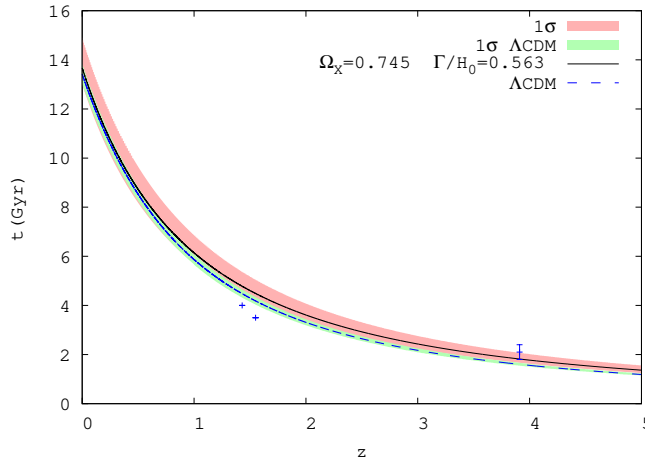


Figure 4: Dependence of the age of the Universe on redshift for the holographic model (solid line) and the  $\Lambda$ CDM model (dashed line). Also shown are the ages and redshifts of three old luminous objects, namely: galaxies LBDS 53W069, and LBDS 53091, and the quasar APM 08279+5255 - the latter with its  $1\sigma$  error bar. In plotting the curves we have used the best fit value  $H_0 = 68.1 \pm 2.1$  km/s/Mpc for the holographic model and  $H_0 = 72.1^{+1.8}_{-1.9}$  km/s/Mpc for the  $\Lambda$ CDM model.

### III. OBSERVATIONAL CONSTRAINTS

In this section we constrain the three free parameters ( $\Omega_X$ ,  $\Gamma/H_0$ , and  $H_0$ ) of the holographic model presented above with observational data from SN Ia (557 data points), the CMB-shift, BAO, and gas mass fractions in galaxy clusters as inferred from x-ray data (42 data points), and the Hubble rate (15 data points) to obtain the best fit values. As the likelihood function is defined by  $\mathcal{L} \propto \exp(-\chi^2/2)$  the best fit follows from minimizing the sum  $\chi_{\text{total}}^2 = \chi_{\text{sn}}^2 + \chi_{\text{cmb}}^2 + \chi_{\text{bao}}^2 + \chi_{\text{x-rays}}^2 + \chi_{\text{Hubble}}^2$ .

#### A. SN Ia

We contrast the theoretical distance modulus

$$\mu_{th}(z_i) = 5 \log_{10} \left( \frac{D_L}{10 \text{pc}} \right) + \mu_0, \quad (10)$$

where  $\mu_0 = 42.38 - 5 \log_{10} h$ , with the observed distance modulus  $\mu_{obs}(z_i)$  of the 557 supernovae type Ia assembled in the Union2 compilation [7]. The latter data set is substantially richer than previous SN Ia compilations and presents other advantages; mainly, the refitting of all light curves with the SALT2 fitter and an upgraded control of systematic errors. In (10)  $D_L = (1+z) \int_0^z \frac{dz'}{E(z'; \mathbf{p})}$  is the Hubble-free luminosity distance, with  $\mathbf{p}$  the model parameters ( $\Omega_X$ ,  $\Gamma/H_0$ , and  $H_0$ ), and  $E(z; \mathbf{p}) := H(z; \mathbf{p})/H_0$ .

The  $\chi^2$  from the 557 SN Ia is given by

$$\chi_{sn}^2(\mathbf{p}) = \sum_{i=1}^{557} \frac{[\mu_{th}(z_i) - \mu_{obs}(z_i)]^2}{\sigma^2(z_i)}, \quad (11)$$

where  $\sigma_i$  stands for the  $1\sigma$  uncertainty associated to the  $i$ th data point.

To eliminate the effect of the nuisance parameter  $\mu_0$ , which is independent of the data points and the data set, we follow the procedure of [37] and obtain  $\tilde{\chi}_{sn}^2 = \chi_{sn}^{2(\text{minimum})} = 569.497$ .

## B. CMB shift

The CMB shift parameter measures the displacement of the first acoustic peak of the CMB temperature spectrum with respect to the position it would occupy if the Universe were accurately described by the Einstein-de Sitter model. It is approximately model-independent and given by [38, 39]

$$\mathcal{R} = \sqrt{\Omega_{M_0}} \int_0^{z_{rec}} \frac{dz}{E(z; \mathbf{p})}, \quad (12)$$

where  $z_{rec} \simeq 1089$  is the redshift at the recombination epoch. The 7-year WMAP data yields  $\mathcal{R}(z_{rec}) = 1.725 \pm 0.018$  [6]. The best fit value of the model is  $\mathcal{R}(z_{rec}) = 1.753_{-0.027}^{+0.033}$ . Minimization of

$$\chi_{cmb}^2(\mathbf{p}) = \frac{(\mathcal{R}_{th} - \mathcal{R}_{obs})^2}{\sigma_{\mathcal{R}}^2} \quad (13)$$

produces  $\chi_{CMB-shift}^{2(\text{minimum})} = 2.385$ .

## C. BAO

Baryon acoustic oscillations can be traced to pressure waves at the recombination epoch generated by cosmological perturbations in the primeval baryon-photon plasma. They have been

revealed by a distinct peak in the large scale correlation function measured from the luminous red galaxies sample of the Sloan Digital Sky Survey (SDSS) at  $z = 0.35$  [40], as well as in the Two Degree Field Galaxy Redshift Survey (2dFGRS) at  $z = 0.2$  [41]. The peaks can be associated to expanding spherical waves of baryonic perturbations. Each peak introduces a characteristic distance scale

$$D_v(z_{BAO}) = \left[ \frac{z_{BAO}}{H(z_{BAO})} \left( \int_0^{z_{BAO}} \frac{dz}{H(z)} \right)^2 \right]^{\frac{1}{3}} \quad (14)$$

(see Ref. [42] for a pedagogical derivation of this expression).

Data from SDSS and 2dFGRS measurements yield  $D_v(0.35)/D_v(0.2) = 1.736 \pm 0.065$  [41]. The best fit value for the holographic model is  $D_v(0.35)/D_v(0.2) = 1.642 \pm 0.003$ , and minimization of

$$\chi_{bao}^2(\mathbf{p}) = \frac{([D_v(0.35)/D_v(0.2)]_{th} - [D_v(0.35)/D_v(0.2)]_{obs})^2}{\sigma_{D_v(0.35)/D_v(0.2)}^2} \quad (15)$$

gives  $\chi_{bao}^{2(\text{minimum})} = 2.089$ .

#### D. Gas mass fraction

Since the bulk of baryons in galaxy clusters are in the form of hot x-ray emitting gas clouds (other baryon sources lagging far behind in mass) the fraction of baryons in clusters,  $f_{gas} := M_{gas}/M_{tot}$ , results of prime interest for it seems a good indicator of the overall cosmological ratio  $\Omega_{baryons}/\Omega_M$  and, up to a fair extent, it is independent of redshift [43]. The aforesaid fraction is related to the cosmological parameters through  $f_{gas} \propto d_A^{3/2}$ , where

$d_A := (1+z)^{-1} \int_0^z \frac{dz'}{H(z')}$  stands for the angular diameter distance to the cluster.

We used 42 Chandra measurements of dynamically relaxed galaxy clusters in the redshift interval  $0.05 < z < 0.1$  [44]. To fit the data we have employed the empirical formula

$$f_{gas}(z) = \frac{K A \gamma b(z)}{1 + s(z)} \frac{\Omega_{B0}}{\Omega_{M0}} \left( \frac{d_A^{\Lambda CDM}}{d_A} \right)^{3/2} \quad (16)$$

(see Eq. (3) in Ref. [44]) in which the  $\Lambda$ CDM model is utilized as reference. Here, the parameters  $K$ ,  $A$ ,  $\gamma$ ,  $b(z)$  and  $s(z)$  model the amount of gas in the clusters. We fix these parameters to their respective best fit values which can be found in Ref. [44].

The  $\chi^2$  function from the 42 galaxy clusters reads

$$\chi_{x-rays}^2(\mathbf{p}) = \sum_{i=1}^{42} \frac{([f_{gas}(z_i)]_{th} - [f_{gas}(z_i)]_{obs})^2}{\sigma^2(z_i)}, \quad (17)$$

and its minimum value results to be  $\chi_{x\text{-rays}}^{2(\text{minimum})} = 44.758$ .

Figure 5 shows the fit to the data.

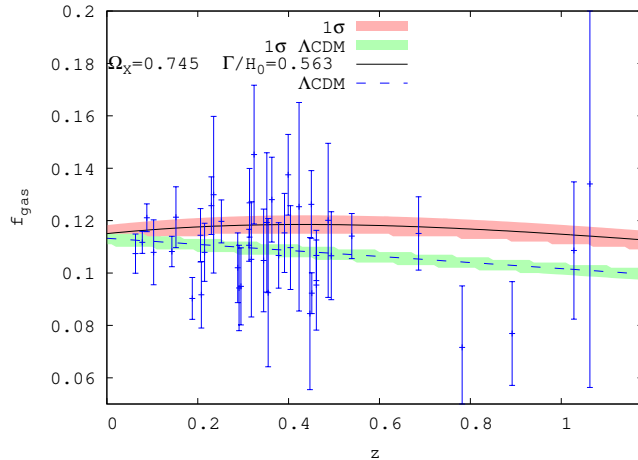


Figure 5: Gas mass fraction in 42 relaxed galaxy clusters vs. redshift. The solid and dashed curves correspond to the best fit models: holographic and  $\Lambda$ CDM, respectively. The data points with their error bars are taken from Table III in Ref. [44].

### E. History of the Hubble parameter

The history of the Hubble parameter,  $H(z)$ , is poorly constrained though, recently, some high precision measurements by Riess *et al.* at  $z = 0$ , obtained from the observation of 240 Cepheid variables of rather similar periods and metallicities [45], and Gaztañaga *et al.*, at  $z = 0.24, 0.34,$  and  $0.43$  [46], who used the BAO peak position as a standard ruler in the radial direction, have improved matters somewhat. To constrain the model we have employed these four data alongside 11 less precise data, in the redshift interval  $0.1 \lesssim z \lesssim 1.8$ , from Simon *et al.* [47] and Stern *et al.* [48], derived from the differential ages of passive-evolving galaxies and archival data.

Minimization of

$$\chi_{Hubble}^2(\mathbf{p}) = \sum_{i=1}^{15} \frac{[H_{th}(z_i) - H_{obs}(z_i)]^2}{\sigma^2(z_i)} \quad (18)$$

provided us with  $\chi_{Hubble}^{2(\text{minimum})} = 11.897$  and  $H_0 = 68.1 \pm 2.1$  km/s/Mpc as the best fit for the Hubble's constant. Figure 6 depicts the Hubble history according to the best fit holographic model alongside the best  $\Lambda$ CDM model.

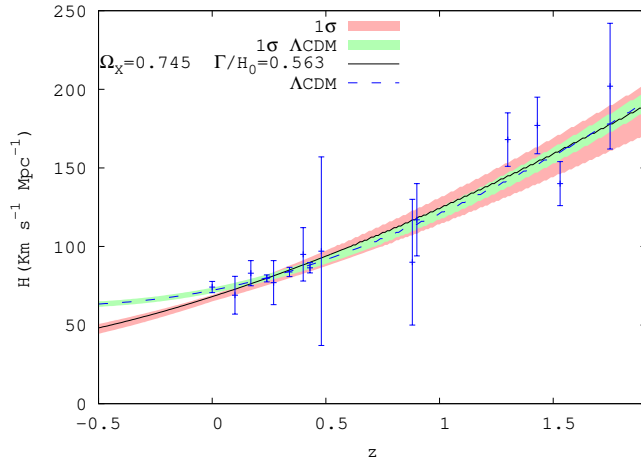


Figure 6: Plot of  $H(z)$  for the best fit values of the holographic model (solid line) and the  $\Lambda$ CDM model (dashed line). The data points and error bars are borrowed from Refs. [45–47].

Figures 7 and 8 summarize our analysis. The left panel of Fig. 7 depicts the 68.3% and 95.4% confidence contours for SN Ia (orange), CMB shift (brown), BAO (blue), x-ray (black), and  $H(z)$  (green), in the  $(\Omega_X, \Gamma/H_0)$  plane. The joined constraints corresponding to  $\chi_{total}^2$  are shown as shaded contours. The right panel depicts the 68.3% and 95.4% confidence regions in the  $(\Omega_{X0}, H_0)$  plane of the holographic model (shaded regions) and the  $\Lambda$ CDM model (blue contours). As it is apparent, the models present a non-small overlap at  $2\sigma$  level.

Figure 8 depicts the normalized likelihoods,  $\mathcal{L} \propto \exp(-\chi_{total}^2/2)$ , of the three free parameters of the holographic model.

Altogether, by constraining the holographic model presented in Section II with SN Ia, CMB-shif, BAO, x-rays, and  $H(z)$  data we obtain  $\Omega_X = 0.745 \pm 0.007$ ,  $\Gamma/H_0 = 0.563_{-0.015}^{+0.017}$ , and  $H_0 = 68.1 \pm 2.1$  km/s/Mpc as best fit parameters, with  $\chi_{total}^2 = 630.627$ . This value lies well inside the  $1\sigma$  interval ( $\chi_{total}^2/dof \approx 1.03$ ). It should be noted that the no interacting case is discarded at very high confidence level. This means no surprise at all since for  $\Gamma = 0$  the model reduces to the Einstein-de Sitter ( $\Omega_M = 1, \Omega_X = 0$ ) and accordingly, as Eq. (8) tells us, the transition from deceleration to acceleration cannot occur.

Table I shows the partial, total, and total  $\chi^2$  over the number of degrees of freedom of the holographic model along with the corresponding values for the  $\Lambda$ CDM model. In the latter one has just two free parameters,  $\Omega_{M0}$  and  $H_0$ . Their best fit values after constraining the model to the data are  $\Omega_{M0} = 0.259_{-0.005}^{+0.006}$ , and  $H_0 = 72.1_{-1.9}^{+1.8}$  km/s/Mpc, with  $\chi_{total}^2 = 593.142$ .

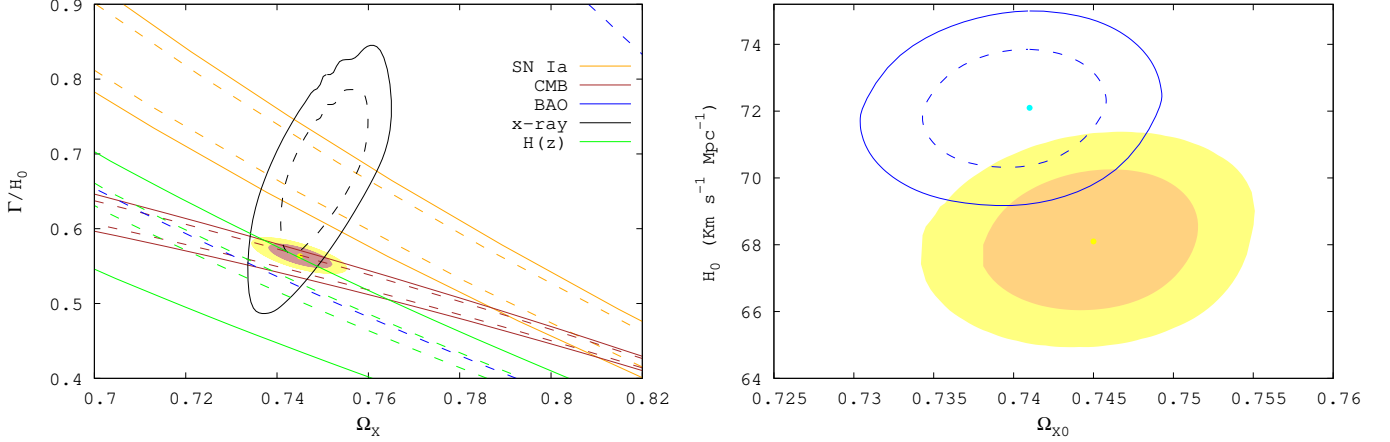


Figure 7: Left panel: the 68.3% and 95.4% confidence contours for the pair of free parameters  $(\Omega_X, \Gamma/H_0)$  obtained by constraining the holographic model with SN Ia+CMB-shift+ BAO+x-ray+H(z) data. The joined constraints corresponding to  $\chi^2_{total}$  are rendered as shaded contours. The no interacting case is largely disfavored by the data. Right panel: the 68.3% and 95.4% confidence contours for the pair  $(\Omega_{X0}, H_0)$  of the holographic model (shaded contours) and the  $\Lambda$ CDM model (blue contours). The solid points signal the location of the best fit values. Notice the overlap at  $2\sigma$  confidence level between both models.

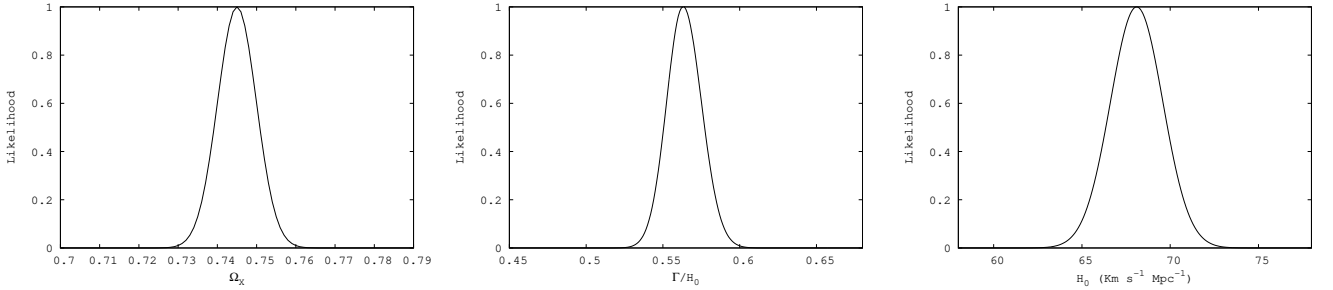


Figure 8: The normalized likelihoods of  $\Omega_X$ ,  $\Gamma/H_0$ , and  $H_0$ .

We see that the  $\Lambda$ CDM model fits the data better than the holographic model in spite of having one parameter less. Thus, the former model should be preferred on statistical grounds. Nevertheless, this does not tell the whole story; the  $\Lambda$ CDM cannot address the cosmic coincidence problem and has some tension with the age of the old quasar APM 08279+5255. By contrast, the holographic model answers the said problem and shows compatibility, at  $1\sigma$ , with the age of the old quasar.

Model	$\chi_{sn}^2$	$\chi_{cmb}^2$	$\chi_{bao}^2$	$\chi_{x-rays}^2$	$\chi_H^2$	$\chi_{total}^2$	$\chi_{total}^2/dof$
Holographic	569.497	2.385	2.089	44.758	11.897	630.627	1.03
$\Lambda$ CDM	541.833	0.013	1.047	41.527	8.727	593.142	0.97

Table I:  $\chi^2$  values for the best fit holographic model ( $\Omega_X = 0.745 \pm 0.007$ ,  $\Gamma/H_0 = 0.563_{-0.015}^{+0.017}$ , and  $H_0 = 68.1 \pm 2.1$  km/s/Mpc), and the best fit  $\Lambda$ CDM model ( $\Omega_{M0} = 0.259_{-0.005}^{+0.006}$ , and  $H_0 = 72.1_{-1.9}^{+1.8}$  km/s/Mpc).

#### IV. EVOLUTION OF THE GROWTH FUNCTION

It is not unfrequent to find in the literature cosmological models that differ greatly on their basic assumptions but, nevertheless, present a rather similar dynamical behavior. It is, therefore, rather hard to discriminate them at the background level. However, their differences are more readily manifested at the perturbative level (though, admittedly, the uncertainty in the corresponding data are, in general, wider). This justifies our interest in studying the evolution of the matter perturbations of the holographic model inside the horizon.

A prime tool in this connection is the growth function, defined as

$$f := d \ln \delta_M / d \ln a, \quad (19)$$

where  $\delta_M$  denotes the density contrast of matter. In order to derive an evolution equation for  $f$ , we start from the energy balance for the matter component in the Newtonian approximation

$$\dot{\delta}_M - \frac{k^2}{a^2} v_M = -\frac{Q}{\rho_M} \delta_M + \frac{\hat{Q}}{\rho_M}. \quad (20)$$

Here,  $v_M$  is the velocity potential, defined by  $\hat{u}_{M\alpha} \equiv v_{M,\alpha}$ , where  $u_{M\alpha}$  is the matter four-velocity, and the hat means perturbation of the corresponding quantity.

Recalling Eqs. (4) and (5) and that  $\Gamma$  and  $r$  do not vary, we can write

$$\dot{\delta}_M - \frac{k^2}{a^2} v_M = -\frac{\Gamma}{r} (\delta_M - \delta_X). \quad (21)$$

Usually, the density contrast of dark energy is neglected under the assumption that dark energy does not cluster on small scales. However, as forcefully argued by Park *et al.* [49], the neglecting of  $\delta_X$  can be fully justified in the case of the cosmological constant only. At any rate, in the present case the setting of  $\delta_X$  to zero would be incorrect given the coupling between both energy components at the background level (i.e., Eqs. (4)). It seems therefore reasonable to include a coupling, at least approximately, also at the perturbative level. The simplest possibility is to

assume a proportionality  $\delta_X = \alpha \delta_M$  with a constant  $\alpha$ . As we shall see, the only consistent choice for this constant (under the conditions that  $\Gamma$  and  $r$  are held fixed) is  $\alpha = 1$ . Thus, Eq. (21) becomes

$$\dot{\delta}_M - \frac{k^2}{a^2} v_M = -\frac{\Gamma}{r} (1 - \alpha) \delta_M. \quad (22)$$

An equation for  $v_M$  follows from the momentum conservation of the matter component. Assuming that there is no source term in the matter rest frame, this equation takes the simple form

$$\dot{v}_M + \phi = 0, \quad (23)$$

where  $\phi$  is the Newtonian potential. Differentiation of (22), use of (23) and (22), and substitution of the scale factor for the time as independent variable, leads to

$$\delta_M'' + \frac{3}{2a} \left[ 1 + \frac{\Gamma}{3Hr} + \frac{2(1-\alpha)}{3} \frac{\Gamma}{Hr} \right] \delta_M' - \frac{3}{2a^2} \frac{r+\alpha}{r+1} \left[ 1 - \frac{4(1-\alpha)}{3} \frac{\Gamma}{Hr} \frac{r+1}{r+\alpha} \right] \delta_M = 0, \quad (24)$$

where use of Friedmann's equation,  $4\pi G\rho_m = \frac{3}{2}H^2 \frac{r}{1+r}$ , has been made; the prime means derivative with respect to  $a$ .

For a vanishing  $\Gamma$  we must recover the conventional perturbation equation  $\delta_M'' + \frac{3}{2a}\delta_M' - \frac{3}{2a^2}\delta_M = 0$  with the growing solution  $\delta_M \propto a$  for a dust universe. Clearly, this is only feasible for  $\alpha = 1$ . With this choice the fractional matter perturbation  $\delta_M$  coincides with the total fractional energy density perturbation,  $\delta \equiv \frac{\hat{\rho}_M + \hat{\rho}_X}{\rho_M + \rho_X}$ . It follows that the basic matter perturbation equation for the interacting holographic models reduces to

$$\delta_M'' + \frac{3}{2a} \left[ 1 + \frac{\Gamma}{3Hr} \right] \delta_M' - \frac{3}{2a^2} \delta_M = 0. \quad (25)$$

Replacing  $\delta_M$  by the growth function  $f$ , last equation becomes

$$f' + f^2 + \frac{1}{2} \left( 1 + \frac{\Gamma}{Hr} \right) f - \frac{3}{2} = 0 \quad (26)$$

with  $f' := df/d\ln a$ . This has the advantage of being a first order differential equation. Notice that in the absence of interaction,  $\Gamma = 0$ , its solution is simply  $f = 1$  as it should, i.e., a dust dominated universe.

Figure 9 depicts the evolution of the growth function in terms of the redshift for the holographic as well as for the  $\Lambda$ CDM model. The latter appears to fit the data below  $z \simeq 0.6$  better than the former. In particular, at  $z = 0.15$  the best fit holographic model deviates  $\Delta f = 0.3$  (corresponding to  $3\sigma$ ) from the observed value (though it falls within  $1\sigma$  with the remaining data points) while the best fit  $\Lambda$ CDM model falls within  $1\sigma$  also at  $z = 0.15$ .

At any rate, it has been recently pointed out, from the observation of nearby galaxies, that structure formation must have proceeded faster than predicted by the  $\Lambda$ CDM model [51]. Clearly, slightly enhanced values of  $f$  at low redshifts helps accelerate the formation of galaxies and clusters thereof.

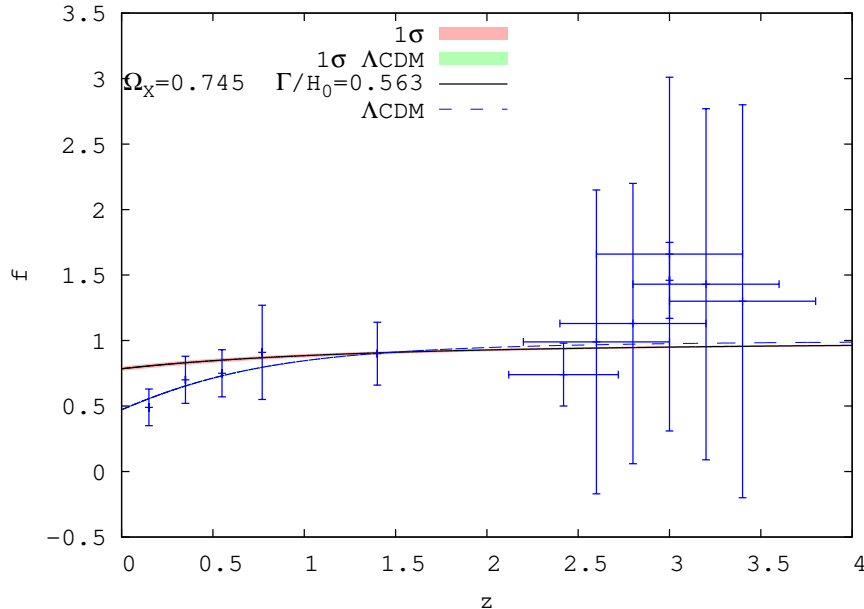


Figure 9: Growth function vs. redshift for the best fit holographic model (solid line). Also shown is the prediction of the  $\Lambda$ CDM model (dashed line). The observational data are borrowed from Table II in Ref. [50]. In plotting the curves no fit to these data was made.

## V. CONCLUDING REMARKS

We constrained the interacting holographic model of Section II with data from SN Ia, CMB shift, BAO, the gas mass fraction in galaxy clusters, and  $H(z)$ . The parameters of the best fit model are:  $\Omega_X = 0.745 \pm 0.007$ ,  $\Gamma/H_0 = 0.563^{+0.017}_{-0.015}$ , and  $H_0 = 68.1 \pm 2.1$  km/s/Mpc. We have not included data of the growth function in the likelihood analysis given the wide uncertainties of the current data. However, we have derived the differential equation for  $f$ , Eq. (26), and integrated it numerically for the best fit model.

It conforms reasonably well to the observational data but not so well as the  $\Lambda$ CDM model (best fit values:  $\Omega_{M0} = 0.259^{+0.006}_{-0.005}$ ,  $H_0 = 72.1^{+1.8}_{-1.9}$  km/s/Mpc) does notwithstanding the latter has one less free parameter than the former. However, the holographic model greatly alleviates the cosmic coincidence problem and seems compatible at  $1\sigma$  level with the age of the old quasar

APM 08279+5255. Besides, the observational data from the CMB shift, BAO, x-ray, and some of the  $H(z)$  data, are not fully model independent owing to the fact that they are extracted with the help of the conventional  $\Lambda$ CDM. This frequently makes the latter tend to be observationally favored over any other cosmological model. Moreover, the BAO data are conventionally determined under the assumption of purely adiabatic perturbations. However, as recently argued [52], should isocurvature components be present the shape and location of the CMB acoustic peaks would be altered and the data extracted from BAO affected.

Clearly, we must wait for more abundant, varied, and model-independent accurate data to tell which of the two models survives. If eventually neither of the two does, we should not be so much disenchanted because, at any rate, this “negative” result would have narrowed significantly the parameter space of dark energy.

### Acknowledgments

We are indebted to Fernando Atrio-Barandela for helpful comments on an earlier draft of this paper. ID research was funded by the “Universidad Autónoma de Barcelona” through a PIF fellowship. DP is grateful to the “Departamento de Física de la Universidade Federal do Espirito Santo”, where part of this work was done, for financial support and warm hospitality. This research was partly supported by the Spanish Ministry of Science and Innovation under Grant FIS2009-13370-C02-01, and the “Direcció de Recerca de la Generalitat” under Grant 2009SGR-00164. Also, this work was partially funded by CNPq (Brazil) and FAPES (Brazil).

- 
- [1] W. Zimdahl and D. Pavón, *Class. Quantum Grav.* **24**, 5461 (2007).
  - [2] A. G. Cohen, D.B. Kaplan and A.E. Nelson, *Phys. Rev. Lett.* **82**, 4971 (1999).
  - [3] M. Li, *Phys. Lett. B* **603**, 1 (2004).
  - [4] A.G. Riess *et al.*, *Astrophys. J.* **116**, 1009 (1998).
  - [5] S. Perlmutter *et al.*, *Astrophys. J.* **517**, 565 (1999).
  - [6] E. Komatsu *et al.*, astro-ph/1001.4538. (2010).
  - [7] R. Amanullah *et al.* (The Supernova Cosmology Project), *Astrophys. J.* (in the press), arXiv:1004.1711.
  - [8] D. Pavón and W. Zimdahl, *Phys. Lett. B* **628**, 206 (2005).
  - [9] B. Wang, Y.G. Gong, and E. Abdalla, *Phys. Lett. B* **624**, 141 (2005).
  - [10] B. Wang, C.-Y. Lin, and E. Abdalla, *Phys. Lett. B* **637**, 357 (2006).
  - [11] M.R. Setare, J. Zhang, and X. Zhang, *JCAP*03 (2007) 007.

- [12] M. Li, X.-D. Li, S. Wang, Y. Wang, and X. Zhang, JCAP12 (2009) 014.
- [13] S.M.R. Micheletti, JCAP05 (2010) 009.
- [14] C. Gao, F. Wu, X. Chen, and Y. G. Shen, Phys. Rev. D 79, 043511 (2009).
- [15] M. Suwa and T. Nihei, Phys. Rev. D 81, 023519 (2010).
- [16] L. Xu, W. Li, and J. Lu, Modern. Phys. Lett. A 17, 1355 (2009).
- [17] L. Xu and Y. Wang, JCAP06 (2010) 002.
- [18] S. D. H. Hsu, Phys. Lett. B 594, 13 (2004).
- [19] D. Pavón and B. Wang, Gen. Relativ. Grav. 41, 1 (2009).
- [20] E. Abdalla, L.R. Abramo, and J.C.C. Souza, arXiv:0910.5236.
- [21] C. Wetterich, Nucl. Phys. B 302, 668 (1988); *ibid.* Astron. Astrophys. 301, 321 (1995).
- [22] L. Amendola, Phys. Rev. D 62, 043511 (2010); L. Amendola and D. Tocchini-Valentini, Phys. Rev. D 64, 043509 (2001).
- [23] L.P. Chimento, A.S. Jakubi, D. Pavón, and W. Zimdahl, Phys. Rev. D., Phys. Rev. D 67, 083513 (2003).
- [24] Ph. Brax and J. Martin, JCAP11 (2006) 008.
- [25] Jérôme Martin, personal communication.
- [26] S. del Campo, R. Herrera, and D. Pavón, Phys. Rev. D 78, 021302(R) (2008); *ibid.* JCAP01 (2009) 020.
- [27] M.C. Bento, O. Bertolami, and A.A. Sen, Phys. Rev. D 66, 043507 (2002).
- [28] P. Serra *et al.*, Phys. Rev. D 80, 121302 (2009).
- [29] R.A. Daly, S.G. Djorgovski, K.A. Freeman, M. Mory C.P. O’Dea, P. Kharb, and S. Baum, Astrophys. J. 677, 1 (2008).
- [30] J. Dunlop *et al.*, “Old Stellar Populations in Distant Radio Galaxies”, in *The Most Distant Radio Galaxies*, eds. H.J.A. Rottgering, P. Best and M.D. Lehnert (Kluwer, Dordrecht, 1999), p. 71.
- [31] J. Dunlop *et al.*, Nature (London) 381, 581 (1996).
- [32] H. Spinrad *et al.*, Astrophys. J. 484, 581 (1997).
- [33] G. Hasinger *et al.*, Astrophys. J. 573, L77 (2002); S. Komossa and G. Hasinger, in Proc. of the Workshop “XEUS -studying the evolution of the hot universe”, eds. G. Hasinger *et al.*, astro-ph/0207321.
- [34] A.C.S. Friaca, J.S. Alcaniz, and J.A.S. Lima, Mon. Not. R. Astron. Soc. 362, 1295 (2005).
- [35] H. Wei and S.N. Zhang, Phys. Rev. D 76, 063003 (2007).
- [36] J. Cui and X. Zhang, Phys. Lett. B 690, 233 (2010).
- [37] S. Nesseris and L. Perivolaropoulos, Phys. Rev. D 72, 123519 (2005).
- [38] Y. Wang and P. Mukherjee, Astrophys. J. 650, 1 (2006).
- [39] J.R. Bond, G. Efstathiou, and M. Tegmark, Mon. Not. R. Astron. Soc. 291, L33 (1997).
- [40] D.J. Eisenstein *et al.* [DSS Collaboration], Astrophys. J. 633, 560 (2005).
- [41] W.J. Percival *et al.*, Mon. Not. R. Astron. Soc. 401, 2148 (2010).
- [42] S. Nesseris and L. Perivolaropoulos, JCAP01 (2007) 018.

- [43] S.M.D. White, J. F. Navarro, A. Evrard, and C.S. Frenk, *Nature* 366, 429 (1993).
- [44] S.W. Allen *et al.*, *Mon. Not. R. Astron. Soc.* 383, 879 (2008).
- [45] A.G. Riess, *et al.*, *Astrophys. J.* 699, 539 (2009).
- [46] E. Gaztañaga, A. Cabré, and L. Hui, *Mon. Not. R. Astron. Soc.* 399, 1663 (2009).
- [47] J. Simon, L. Verde, and R. Jiménez, *Phys. Rev. D* 71, 123001 (2005).
- [48] D. Stern, R. Jiménez, L. Verde, M. Kamionkowski, and S.A. Stanford, *JCAP*02 (2010) 008.
- [49] C.-G. Park, J. Hwang, J. Lee, and H. Noh, *Phys. Rev. Lett.* 103, 151303 (2009).
- [50] Y. Gong, *Phys. Rev. D* 78, 123010 (2008).
- [51] P.J.E. Peebles and A. Nusser, *Nature* 465, 565 (2010).
- [52] A. Mangilli, L. Verde, and M. Beltran, arXiv:1006.3806 [astro-ph.CO].